EURASIP Journal on Wireless Communications and Networking
a SpringerOpen Journal

RESEARCH Open Access

Interference-aware receiver structure for multi-user MIMO and LTE

Rizwan Ghaffar* and Raymond Knopp

Abstract

In this paper, we propose a novel low-complexity interference-aware receiver structure for multi-user MIMO that is based on the exploitation of the structure of residual interference. We show that multi-user MIMO can deliver its promised gains in modern wireless systems in spite of the limited channel state information at the transmitter (CSIT) only if users resort to intelligent interference-aware detection rather than the conventional single-user detection. As an example, we focus on the long term evolution (LTE) system and look at the two important characteristics of the LTE precoders, i.e., their low resolution and their applying equal gain transmission (EGT). We show that EGT is characterized by full diversity in the single-user MIMO transmission but it loses diversity in the case of multi-user MIMO transmission. Reflecting on these results, we propose a LTE codebook design based on two additional feedback bits of CSIT and show that this new codebook significantly outperforms the currently standardized LTE codebooks for multi-user MIMO transmission.

1. Introduction

The spatial dimension surfacing from the usage of multiple antennas promises improved reliability, higher spectral efficiency [1], and the spatial separation of users [2]. This spatial dimension (MIMO) is particularly beneficial for precoding in the downlink of multi-user cellular systems (broadcast channel), where these spatial degrees of freedom at the transmitter can be used to transmit data to multiple users simultaneously. This is achieved by creating independent parallel channels to the users (canceling multi-user interference) and the users subsequently employ simplified single-user receiver structures. However, the transformation of cross-coupled channels into parallel non-interacting channels necessitates perfect channel state information at the transmitter (CSIT) whose acquisition in a practical system, in particular frequency division duplex (FDD) system, is far from realizable. This leads to the precoding strategies based on the partial or quantized CSIT [3], which limit the gains of multi-user MIMO.

Ongoing standardizations of modern cellular systems are investigating different precoding strategies based on low-level quantized CSIT to transmit spatial streams to multiple users sharing the same time-frequency resources. In third-generation partnership project long-term evolution (3GPP LTE) system [4], the CSIT acquisition is based on the precoder codebook approach. These LTE precoders are characterized by low resolution and are further based on the principle of equal gain transmission (EGT). These precoders when employed for the multi-user MIMO mode of transmission are unable to cancel the multi-user interference thereby increasing the sub-optimality of conventional single-user detection. This has led to the common perception that multi-user MIMO mode is not workable in LTE [[5], p. 244].

Considering multi-user detection, we propose in this paper a low-complexity interference-aware receiver [6] for the multi-user MIMO in LTE. Though multi-user detection has been extensively investigated in the literature for the uplink (multiple access channel), its related complexity has so far prohibited its employment in the downlink (broadcast channel). For the multiple access channel, several multi-user detection techniques exist in the literature starting from the optimal multi-user receivers [7] to their near-optimal reduced complexity counterparts (sphere decoders [8]). The complexity associated with these techniques led to the investigation of low-complexity solutions as sub-optimal linear multi-user receivers [9], iterative multi-user receivers [10,11], and decision-feedback receivers [12,13]. Since in

* Correspondence: rizwan.ghaffar@eurecom.fr
Eurecom, 2229 route des Crêtes, B.P.193, Sophia Antipolis Cedex, 06904, France

practice, most wireless systems employ error control coding combined with the interleaving, recent work in this area has addressed multi-user detection for coded systems based on soft decisions [14,15].

Our proposed low-complexity interference-aware receiver structure not only reduces one complex dimension of the system but is also characterized by exploiting the interference structure in the detection process. Considering this receiver structure, we investigate the effectiveness of the low-resolution LTE precoders for the multi-user MIMO mode and show that multi-user MIMO can bring significant gains in future wireless systems if the users resort to intelligent interference-aware detection as compared to the sub-optimal single-user detection. We further look at the second characteristic of the LTE precoders, i.e., EGT both for the single-user and multi-user MIMO modes. We show that the EGT has full diversity in the single-user MIMO mode (a result earlier derived for equal gain combining for BPSK in [16] and for EGT in MIMO systems in [17]); however, it suffers from a loss of diversity in multi-user MIMO mode [18]. Based on this analysis, we propose a design criteria for the precoder codebooks and show that the additional feedback of two bits for CSIT can lead to significant improvement in the performance of the multi-user MIMO.

Regarding notations, we will use lowercase or uppercase letters for scalars, lowercase boldface letters for vectors and uppercase boldface letters for matrices. The matrix $\mathbf{I}_n$ is the $n \times n$ identity matrix. $|.|$ and $||.||$ indicate norm of scalar and vector while $(.)^T$, $(.)^*$, and $(.)^\dagger$ indicate transpose, conjugate, and conjugate transpose, respectively. $(.)_R$ indicates the real part and $(.)_I$ indicates the imaginary part of a complex number. The notation $E(.)$ denotes the mathematical expectation while $Q(y) = \frac{1}{\sqrt{2\pi}} \int_y^\infty e^{-x^2/2} \mathrm{d}x$ denotes the Gaussian Q-function. All logarithms are to the base 2.

The paper is divided into eight sections. In Sec. II, we give a brief overview of LTE and define the system model. In Sec. III, we consider a geometric scheduling strategy for the multi-user MIMO mode in LTE and propose a low-complexity interference-aware receiver structure. In Sec. IV, we look at the information theoretic perspective of the proposed receiver structure. Sec. V is dedicated to the performance analysis of the EGT that is followed by the simulation results. Before concluding the paper, we propose a design criteria for the precoder codebooks of the forthcoming standardizations of LTE. The proof details in the paper have been relegated to appendices to keep the subject material simple and clear.

2. LTE system model

A. LTE–A brief overview

In 3GPP LTE, a 2 × 2 configuration for MIMO is assumed as the baseline configuration; however, configurations with four transmit or receive antennas are also foreseen and reflected in the specifications [19]. LTE restricts the transmission of maximum of two codewords in the downlink that can be mapped onto different layers where one codeword represents an output from the channel encoder. Number of layers available for the transmission is equal to the rank of the channel matrix (maximum 4). In this paper, we restrict ourselves to the baseline configuration with the eNodeB (LTE notation for the base station) equipped with two antennas while we consider single and dual-antenna user equipments (UEs). Physical layer technology employed for the downlink in LTE is OFDMA combined with bit interleaved coded modulation (BICM) [20]. Several different transmission bandwidths are possible, ranging from 1.08 to 19.8 MHz with the constraint of being a multiple of 180 kHz. Resource blocks (RBs) are defined as groups of 12 consecutive resource elements (REs - LTE notation for the subcarriers) with a bandwidth of 180 kHz thereby leading to the constant RE spacing of 15 kHz. Approximately, 4 RBs form a subband and the feedback is generally done on subband basis. Seven operation modes are specified in the downlink of LTE; however, we shall focus on the following four modes:

- *Transmission mode 2*. Fall-back transmit diversity. Transmission rank is 1, i.e., one codeword is transmitted by the eNodeB. Employs Alamouti space-time or space-frequency codes [21].
- *Transmission mode 4*. Closed-loop spatial multiplexing. Transmission rank is 2, i.e., two codewords are transmitted by the eNodeB to the UE in the single-user MIMO mode. UEs need to have minimum of two antennas.
- *Transmission mode 5*. Multi-user MIMO mode. Supports only rank-1 transmission, i.e., one codeword for each UE.
- *Transmission mode 6*. Closed-loop precoding for rank-1 transmission, i.e., one codeword for the UE in the single-user MIMO mode.

In the case of transmit diversity and closed-loop precoding, one codeword (data stream) is transmitted to each UE using Alamouti code in the former case and LTE precoders in the latter case. Time-frequency resources are orthogonal to the different UEs in these modes thereby avoiding interference in the system. However, in the multi-user MIMO mode, parallel codewords are transmitted simultaneously, one for each UE, sharing the same time-frequency resources. Note that

LTE restricts the transmission of one codeword to each UE in the multi-user MIMO mode.

For closed-loop transmission modes (mode 4, 5 and 6), precoding mechanisms are employed at the transmit side with the objective of maximizing throughput. The precoding is selected and applied by the eNodeB to the data transmission to a target UE based on the channel feedback received from that UE. This feedback includes a precoding matrix indicator (PMI), a channel rank indicator (RI), and a channel quality indicator (CQI). PMI is an index in the codebook for the preferred precoder to be used by the eNodeB. The granularity for the computation and signaling of the precoding index can range from a couple of RBs to the full bandwidth. For transmission mode 5, the eNodeB selects the precoding matrix to induce high orthogonality between the codewords so that the interference between UEs is minimized. In transmission modes 4 and 6, the eNodeB selects the precoding vector/matrix such that codewords are transmitted to the corresponding UEs with maximum throughput.

In order to avoid excessive downlink signaling, transmission mode for each UE is configured semi-statically via higher layer signaling, i.e., it is not allowed for a UE to be scheduled in one subframe in the multi-user MIMO mode and in the next subframe in the single-user MIMO mode. For the case of eNodeB with two antennas, LTE proposes the use of following four precoders for transmission modes 5 and 6:

$$\mathbf{p} = \left\{ \frac{1}{\sqrt{4}} \begin{bmatrix} 1 \\ 1 \end{bmatrix}, \frac{1}{\sqrt{4}} \begin{bmatrix} 1 \\ -1 \end{bmatrix}, \frac{1}{\sqrt{4}} \begin{bmatrix} 1 \\ j \end{bmatrix}, \frac{1}{\sqrt{4}} \begin{bmatrix} 1 \\ -j \end{bmatrix} \right\} \quad (1)$$

The number of precoders increases to sixteen in the case of four transmit antennas; however, in this paper, we restrict to the case of two transmit antennas. For transmission mode 4, LTE proposes the use of following two precoder matrices on subband basis.

$$\mathbf{P} = \left\{ \frac{1}{\sqrt{4}} \begin{bmatrix} 1 & 1 \\ 1 & -1 \end{bmatrix}, \frac{1}{\sqrt{4}} \begin{bmatrix} 1 & 1 \\ j & -j \end{bmatrix} \right\} \quad (2)$$

Note that there is a possibility of swapping the columns in **P** but the swap must occur over the entire band.

B. System model

We first consider the system model for transmission mode 5, i.e., the multi-user MIMO mode in which the eNodeB transmits one codeword each to two single-antenna UEs using the same time-frequency resources. Transmitter block diagram is shown in Figure 1. During the transmission for UE-1, the code sequence $\underline{\mathbf{c}}_1$ is interleaved by π_1 and is then mapped onto the signal sequence $\underline{\mathbf{x}}_1$. x_1 is the symbol of $\underline{\mathbf{x}}_1$ over a signal set $\chi_1 \subseteq \mathcal{C}$ with a Gray-labeling map where $|\chi_1| = M_1$ and x_2 is the symbol of $\underline{\mathbf{x}}_2$ over signal set χ_2 where $|\chi_2| = M_2$. The bit interleaver for UE-1 can be modeled as π_1: $k' \rightarrow (k, i)$ where k' denotes the original ordering of the coded bits $c_{k'}$, k denotes the RE of the symbol $x_{1,k}$, and i indicates the position of the bit $c_{k'}$ in the symbol $x_{1,k}$. Note that each RE corresponds to a symbol from a constellation map χ_1 for UE-1 and χ_2 for UE-2. Selection of the normal or extended cyclic prefix (CP) for each OFDM symbol converts the downlink frequency-selective channel into parallel flat fading channels.

Cascading IFFT at the eNodeB and FFT at the UE with the cyclic prefix extension, the transmission at the k-th RE for UE-1 in transmission mode 5 can be expressed as

$$y_{1,k} = \mathbf{h}_{1,k}^{\dagger} \mathbf{p}_{1,k} x_{1,k} + \mathbf{h}_{1,k}^{\dagger} \mathbf{p}_{2,k} x_{2,k} + z_{1,k} \quad (3)$$

where $y_{1,k}$ is the received symbol at UE-1 and $z_{1,k}$ is zero mean circularly symmetric complex white Gaussian noise of variance N_0. $x_{1,k}$ is the complex symbol for UE-1 with the variance σ_1^2 and $x_{2,k}$ is the complex symbol for UE-2 with the variance σ_2^2. $\mathbf{h}_{n,k}^{\dagger} \in \mathbb{C}^{1\times 2}$ symbolizes the spatially uncorrelated flat Rayleigh fading MISO channel from eNodeB to the n-th UE (n = 1, 2) at the k-th RE. Its elements can therefore be modeled as independent and identically distributed (iid) zero mean circularly symmetric complex Gaussian random variables with a variance of 0.5 per dimension. Note that $\mathbb{C}^{1\times 2}$ denotes a 2-dimensional complex space. $\mathbf{p}_{n,k}$ denotes the precoding vector for the n-th UE at the k-th RE and is given by (1). For the dual-antenna UEs, the system equation for transmission mode 5 is modified as

$$\mathbf{y}_{1,k} = \mathbf{H}_{1,k}[\mathbf{p}_{1,k} x_{1,k} + \mathbf{p}_{2,k} x_{2,k}] + \mathbf{z}_{1,k} \quad (4)$$

where $\mathbf{y}_{1,k}, \mathbf{z}_{1,k} \in \mathbb{C}^{2\times 1}$ are the vectors of the received symbols and circularly symmetric complex white Gaussian noise of double-sided power spectral density $N_0/2$ at the 2 receive antennas of UE-1, respectively. $\mathbf{H}_{1,k} \in \mathbb{C}^{2\times 2}$ is the channel matrix from eNodeB to UE-1.

In transmission mode 6, only one UE will be served in one time-frequency resource. Therefore, the system equation for single-antenna UEs at the k-th RE is given as

$$y_k = \mathbf{h}_k^{\dagger} \mathbf{p}_k x_k + z_k \quad (5)$$

where $\mathbf{p}_k$ is given by (1). For the dual-antenna UEs, the system equation for mode 6 is modified as

$$\mathbf{y}_k = \mathbf{H}_k \mathbf{p}_k x_k + \mathbf{z}_k \quad (6)$$

3. Multi-user MIMO mode

We now look at the effectiveness of the low-resolution LTE precoders for the multi-user MIMO mode. We

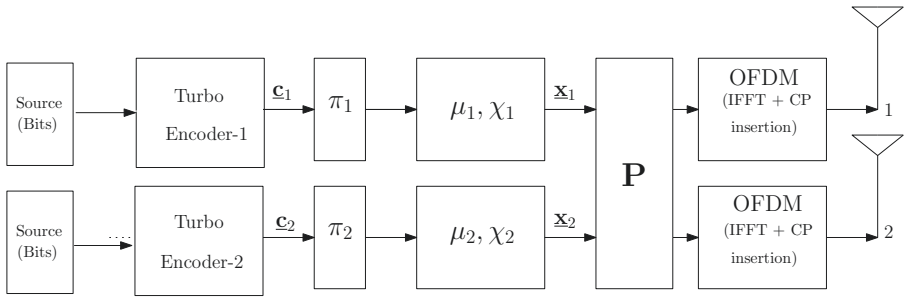

Figure 1 eNodeB in multi-user MIMO mode. π_1 denotes the random interleaver, μ_1 the labeling map and χ_1 the signal set for the codeword of UE-1. P indicates the precoding matrix.

first consider a geometric scheduling strategy [22] based on the selection of UEs with orthogonal precoders.

A. Scheduling strategy

As the processing at the UE is performed on a RE basis for each received OFDM symbol, the dependency on RE index can be ignored for notational convenience. The system equation for the case of single-antenna UEs for the multi-user mode is

$$y_1 = \mathbf{h}_1^\dagger \mathbf{p}_1 x_1 + \mathbf{h}_1^\dagger \mathbf{p}_2 x_2 + z_1 \tag{7}$$

The scheduling strategy is based on the principle of maximizing the desired signal strength while minimizing the interference strength. As the decision to schedule a UE in the single-user MIMO, multi-user MIMO or transmit diversity mode will be made by the eNodeB, each UE would feedback the precoder that maximizes its received signal strength. So this selected precoder by the UE would be the one closest to its matched filter (MF) precoder in terms of the Euclidean distance.

For the multi-user MIMO mode, the eNodeB needs to ensure good channel separation between the co-scheduled UEs. Therefore, the eNodeB schedules two UEs on the same RBs that have requested opposite (orthogonal) precoders, i.e., the eNodeB selects as the second UE to be served in each group of allocatable RBs, one of the UEs whose requested precoder $\mathbf{p}_2$ is 180° out of phase from the precoder $\mathbf{p}_1$ of the first UE to be served on the same RBs. So if UE-1 has requested $\mathbf{p}_1 = \frac{1}{\sqrt{4}}\begin{bmatrix}1\\ q\end{bmatrix}$, $q \in \{\pm 1, \pm j\}$, then eNodeB selects the second UE that has requested $\mathbf{p}_2 = \frac{1}{\sqrt{4}}\begin{bmatrix}1\\ -q\end{bmatrix}$. This transmission strategy also remains valid also for the case of dual-antenna UEs where the UEs feedback the indices of the precoding vectors that maximize the strength of their desired signals, i.e., $||\mathbf{Hp}||^2$. For the multi-user MIMO mode, the eNodeB schedules two UEs on the same RE, which have requested 180° out of phase precoders. The details of this geometric scheduling strategy can be found in [22].

Though this precoding and scheduling strategy would ensure minimization of the interference under the constraint of low-resolution LTE precoders, the residual interference would still be significant. Single-user detection, i.e., Gaussian assumption of the residual interference and its subsequent absorption in noise, would lead to significant degradation in the performance. On the other hand, this residual interference is actually discrete belonging to a finite alphabet and its structure can be exploited in the detection process. However, intelligent detection based on its exploitation comes at the cost of enhanced complexity. Here, we propose a low-complexity interference-aware receiver structure that on one hand reduces one complex dimension of the system while on the other hand, it exploits the interference structure in the detection process.

B. Low-complexity interference-aware receiver

First, we consider the case of single-antenna UEs. Soft decision of the bit $c_{k'}$ of x_1, also known as log-likelihood ratio (LLR), is given as

$$\mathrm{LLR}_1^i\left(c_{k'}|y_1, \mathbf{h}_1^\dagger, \mathbf{P}\right) = \log \frac{p(c_{k'}=1|y_1, \mathbf{h}_1^\dagger, \mathbf{P})}{p(c_{k'}=0|y_1, \mathbf{h}_1^\dagger, \mathbf{P})} \tag{8}$$

We introduce the notation $\Lambda_1^i(y_1, c_{k'})$ for the bit metric that is developed on the lines similar to the (7) and 9 in [20], i.e.,

$$\begin{aligned}\Lambda_1^i(y_1, c_{k'}) &= \log p\left(c_{k'}|y_1, \mathbf{h}_1^\dagger, \mathbf{P}\right)\\ &\approx \log p\left(y_1|c_{k'}, \mathbf{h}_1^\dagger, \mathbf{P}\right)\\ &= \log \sum_{x_1 \in \chi^i_{1,c_{k'}}} \sum_{x_2 \in \chi_2} p(y_1|x_1, x_2, \mathbf{h}_1^\dagger, \mathbf{P})\\ &\approx \min_{x_1 \in \chi^i_{1,c_{k'}}, x_2 \in \chi_2} \frac{1}{N_0}\left|y_1 - \mathbf{h}_1^\dagger \mathbf{p}_1 x_1 - \mathbf{h}_1^\dagger \mathbf{p}_2 x_2\right|^2\end{aligned} \tag{9}$$

where $\chi^i_{1,c_{k'}}$ denotes the subset of the signal set $x_1 \in \chi_1$ whose labels have the value $c_{k'} \in \{0, 1\}$ in the position i. Here, we have used the log-sum approximation, i.e., $\log \sum_j z_j = \max_j \log z_j$ and this bit metric is therefore termed as max-log MAP bit metric. As LLR is the difference of two bit metrics and these will be decoded using a conventional soft-decision Viterbi algorithm, $\frac{1}{N_0}$ (a common scaling factor to all LLRs) can be ignored thereby leading to

$$\begin{aligned}\Lambda^i_1(y_1, c_k) &\approx \min_{x_1 \in \chi^i_{1,c_{k'}}, x_2 \in \chi_2} \left| y_1 - \mathbf{h}^\dagger_1 \mathbf{p}_1 x_1 - \mathbf{h}^\dagger_1 \mathbf{p}_2 x_2 \right|^2 \\ &= \min_{x_1 \in \chi^i_{1,c_{k'}}, x_2 \in \chi_2} \left\{ |y_1|^2 + \left| \mathbf{h}^\dagger_1 \mathbf{p}_1 x_1 \right|^2 + \left| \mathbf{h}^\dagger_1 \mathbf{p}_2 x_2 \right|^2 - 2(\mathbf{h}^\dagger_1 \mathbf{p}_1 x_1 y^*_1)_R + 2(\rho_{12} x^*_1 x_2)_R - 2(\mathbf{h}^\dagger_1 \mathbf{p}_2 x_2 y^*_1)_R \right\} \quad (10)\end{aligned}$$

where $\rho_{12} = \left(\mathbf{h}^\dagger_1 \mathbf{p}_1\right)^* \mathbf{h}^\dagger_1 \mathbf{p}_2$ indicates the cross-correlation between the two effective channels. Here, we have used the relation $|a - b|^2 = |a|^2 + |b|^2 - 2\,(a^*b)_R$ where the subscript $(.)_R$ indicates the real part. Note that the complexity of the calculation of bit metric (10) is $\mathcal{O}(|\chi_1||\chi_2|)$.

In (10), we now introduce two terms as the outputs of MF, i.e., $\bar{y}_1 = \left(\mathbf{h}^\dagger_1 \mathbf{p}_1\right)^* y_1$ and $\bar{y}_2 = \left(\mathbf{h}^\dagger_1 \mathbf{p}_2\right)^* y_1$. Ignoring $|y_1|^2$ (independent of the minimization operation), the bit metric is written as

$$\Lambda^i_1(y_1, c_k) \approx \min_{x_1 \in \chi^i_{1,c_{k'}}, x_2 \in \chi_2} \left\{ \left| \mathbf{h}^\dagger_1 \mathbf{p}_1 x_1 \right| + \left| \mathbf{h}^\dagger_1 \mathbf{p}_2 x_2 \right|^2 - 2(\bar{y}^*_1 x_1)_R + 2\psi_A x_{2,R} + 2\psi_B x_{2,I} \right\} \quad (11)$$

where

$$\psi_A = \rho_{12,R} x_{1,R} + \rho_{12,I} x_{1,I} - \bar{y}_{2,R}$$
$$\psi_B = \rho_{12,R} x_{1,I} - \rho_{12,I} x_{1,R} - \bar{y}_{2,I}$$

Note that the subscript $(.)_I$ indicates the imaginary part.

For x_1 and x_2 belonging to equal energy alphabets, $\left| \mathbf{h}^\dagger_1 \mathbf{p}_1 x_1 \right|^2$ and $\left| \mathbf{h}^\dagger_1 \mathbf{p}_2 x_2 \right|^2$ can be ignored as they are independent of the minimization operation. The values of $x_{2,R}$ and $x_{2,I}$ that minimize Eq. (11) need to be in the opposite directions of ψ_A and ψ_B, respectively, thereby avoiding search on the alphabets of x_2 and reducing one complex dimension in the detection, i.e.,

$$\Lambda^i_1(y_1, c_{k'}) \approx \min_{x_1 \in \chi^i_{1,c_{k'}}} \left\{ -2\bar{y}_{1,R} x_{1,R} - 2\bar{y}_{1,I} x_{1,I} - 2|\psi_A||x_{2,R}| - 2|\psi_B||x_{2,I}| \right\} \quad (12)$$

As an example, we consider the case of QPSK for which the values of $x_{2,R}$ and $x_{2,I}$ are $\left[\pm\frac{\sigma_2}{\sqrt{2}}\right]$, so the bit metric is written as

$$\Lambda^i_1(y_1, c_{k'}) \approx \min_{x_1 \in \chi^i_{1,c_{k'}}} \left\{ -2\bar{y}_{1,R} x_{1,R} - 2\bar{y}_{1,I} x_{1,I} - \sqrt{2}\sigma_2 |\psi_A| - \sqrt{2}\sigma_2 |\psi_B| \right\} \quad (13)$$

For x_1 and x_2 belonging to non-equal energy alphabets, the bit metric is same as (13) but $\left| \mathbf{h}^\dagger_1 \mathbf{p}_1 x_1 \right|^2$ and $\left| \mathbf{h}^\dagger_1 \mathbf{p}_2 x_2 \right|^2$ can no longer be ignored thereby leading to

$$\Lambda^i_1(y_1, c_{k'}) \approx \min_{x_1 \in \chi^i_{1,c_{k'}}} \left\{ \left| \mathbf{h}^\dagger_1 \mathbf{p}_1 \right|^2 |x_{1,R}|^2 + \left| \mathbf{h}^\dagger_1 \mathbf{p}_1 \right|^2 |x_{1,I}|^2 + \left| \mathbf{h}^\dagger_1 \mathbf{p}_2 \right|^2 |x_{2,R}|^2 + \left| \mathbf{h}^\dagger_1 \mathbf{p}_2 \right|^2 |x_{2,I}|^2 - 2\bar{y}_{1,R} x_{1,R} - 2\bar{y}_{1,I} x_{1,I} - 2|\psi_A||x_{2,R}| - 2|\psi_B||x_{2,I}| \right\} \quad (14)$$

Note that the minimization is independent of χ_2 though x_2 appears in the bit metric. The reason of this independence is as follows. The decision regarding the signs of $x_{2,R}$ and $x_{2,I}$ in (14) will be taken in the same manner as for the case of equal energy alphabets. For finding their magnitudes that minimize the bit metric (14), it is the minimization problem of a quadratic function, i.e., differentiating (14) w.r.t $|x_{2,R}|$ and $|x_{2,I}|$ to find the global minima that are given as

$$|x_{2,R}| \rightarrow \frac{|\psi_A|}{\left| \mathbf{h}^\dagger_1 \mathbf{p}_2 \right|^2}, \quad |x_{2,I}| \rightarrow \frac{|\psi_B|}{\left| \mathbf{h}^\dagger_1 \mathbf{p}_2 \right|^2} \quad (15)$$

where $\rightarrow$ indicates the discretization process in which among the finite available points of $x_{2,R}$ and $x_{2,I}$, the point closest to the calculated continuous value is selected. So if x_2 belongs to QAM256, then instead of searching 256 constellation points for the minimization of (14), the metric (15) reduces it to merely two operations thereby trimming down one complex dimension in the detection, i.e., the detection complexity is independent of $|\chi_2|$ and reduces to $\mathcal{O}(|\chi_1|)$.

As a particular example of the discretization of continuous values in (15), we consider the case of x_2 belonging to QAM16. The values of $x_{2,R}$ and $x_{2,I}$ for the case of QAM16 are $\left[\pm\frac{\sigma_2}{\sqrt{10}}, \pm\frac{3\sigma_2}{\sqrt{10}}\right]$ so their magnitudes in (14) are given as

$$\begin{aligned}|x_{2,R}| &= \sigma_2 \frac{1}{\sqrt{10}} \left(2 + (-1)^{I\left(|\psi_A| < \sigma_2 \frac{2\left| \mathbf{h}^\dagger_1 \mathbf{p}_2 \right|^2}{\sqrt{10}} \right)} \right) \\ |x_{2,I}| &= \sigma_2 \frac{1}{\sqrt{10}} \left(2 + (-1)^{I\left(|\psi_B| < \sigma_2 \frac{2\left| \mathbf{h}^\dagger_1 \mathbf{p}_2 \right|^2}{\sqrt{10}} \right)} \right)\end{aligned} \quad (16)$$

and I (.) is the indicator function defined as

$$I(a < b) = \begin{cases} 1 \text{ if } a < b \\ 0 \text{ otherwise} \end{cases}$$

Now we look at the receiver structure for the case of dual-antenna UEs. The system equation for UE-1 (ignoring the RE index) is

$$\mathbf{y}_1 = \mathbf{H}_1[\mathbf{p}_1 x_1 + \mathbf{p}_2 x_2] + \mathbf{z}_1 \quad (17)$$

The receiver structure would remain same with $\mathbf{h}_1^\dagger$ being replaced by $\mathbf{H}_1$, i.e., the channel from eNodeB to the two antennas of UE-1. Subsequently $\bar{y}_1 = (\mathbf{H}_1\mathbf{p}_1)^\dagger \mathbf{y}_1$ and $\bar{y}_2 = (\mathbf{H}_1\mathbf{p}_2)^\dagger \mathbf{y}_1$ are the MF outputs while $\rho_{12} = (\mathbf{H}_1\mathbf{p}_1)^\dagger \mathbf{H}_1\mathbf{p}_2$ is the cross-correlation between two effective channels.

For comparison purposes, we also consider the case of single-user receiver, for which the bit metric is given as

$$\Lambda_1^i(\gamma_1, c_{k'}) \approx \min_{x_1 \in \chi_{i,c_{k'}}^1} \left\{ \frac{1}{(|\rho_{12}|^2\sigma_2^2 + \left|\mathbf{h}_1^\dagger \mathbf{p}_1\right|^2 N_0)} \left| \bar{y}_1 - \left|\mathbf{h}_1^\dagger \mathbf{p}_1\right|^2 x_1 \right|^2 \right\} \quad (18)$$

Table 1 compares the complexities of different receivers in terms of the number of real-valued multiplications and additions for getting all LLR values per RE/subcarrier. Note that n_r denotes the number of receive antennas. This complexity analysis is independent of the number of transmit antennas as the operation of finding effective channels bears same complexity in all receiver structures. Moreover UEs can also directly estimate their effective channels if the pilot signals are also precoded. The comparison shows that the complexity of the interference-aware receiver is of the same order as of single-user receiver while it is far less than the complexity of the max-log MAP receiver. Figure 2 further shows the performance-complexity trade off of different receivers for multi-user MIMO mode in LTE. The performance of the receivers is measured in terms of the SNR at the frame error rate (FER) of 10^{-2} whereas the complexity is determined from Table 1. It shows that the performance of the single-user receiver is severely degraded as compared to that of the interference-aware receiver. In most cases, the single-user receiver fails to achieve the requisite FER in the considered SNR range. On the other hand, interference-aware receiver achieves same performance as max-log MAP receiver but with much reduced complexity.

The interference-aware receiver is therefore not only characterized by low complexity but also resorts to intelligent detection by exploiting the structure of residual interference. Moreover, this receiver structure being based on the MF outputs and devoid of any division operation can be easily implemented in the existing hardware. However, the proposed receiver needs both the channel knowledge and the constellation of interference (co-scheduled UE). As the UE already knows its own channel from the eNodeB and the requested precoder, it can determine the effective channel of the interference based on the geometric scheduling algorithm, i.e., the precoder of the co-scheduled UE is 180° out of phase of its own precoder. Consequently there is no additional complexity in utilizing this receiver structure as compared to using single-user receivers except that the UE needs to know the constellation of interference.

4. Information theoretic perspective

Sum rate of the downlink channel is given as

$$\mathcal{I} = I(Y_1; X_1|\mathbf{h}_1^\dagger, \mathbf{P}) + I(Y_2; X_2|\mathbf{h}_2^\dagger, \mathbf{P}) \quad (19)$$

where $\mathbf{P} = [\mathbf{p}_1 \ \mathbf{p}_2]$ is the precoder matrix, $I\left(Y_1; X_1|\mathbf{h}_1^\dagger, \mathbf{P}\right)$ is the mutual information of UE-1 once it sees interference from UE-2 and $I\left(Y_2; X_2|\mathbf{h}_2^\dagger, \mathbf{P}\right)$ is the mutual information of UE-2 once it sees interference from UE-1. Y_1 is the received symbol at UE-1 while X_1 is the symbol transmitted by the eNodeB to UE-1. Note that interference is present in the statistics of Y_1 and Y_2. No sophisticated power allocation is employed to the two streams as the downlink control information (DCI) in the multi-user mode in LTE includes only 1-bit power offset information, indicating whether a 3 dB transmit power reduction should be assumed or not. We therefore consider equal-power distribution between the two streams. For the calculation of mutual information, we deviate from the unrealistic Gaussian assumption for the alphabets and consider them from discrete constellations. The derivations of the mutual

Table 1 Comparison of receivers complexity

Receiver	Real multiplications	Real additions
Interference-aware receiver (equal energy alphabets)	$8n_r + 2\sqrt{M} + 2M$	$8n_r + 10M + \log(M) - 4$
Interference-aware receiver (non equal energy alphabets)	$12n_r + 4M + \frac{7}{2}\sqrt{M}$	$12n_r + 18M + \log(M) - 6$
Max-log MAP receiver	$2M^2n_r + 8Mn_r$	$6M^2n_r + 4Mn_r + \log(M) - M^2$
Single-user receiver (equal energy alphabets)	$10n_r + 6$	$10n_r - 3$
Single-user receiver (non equal energy alphabets)	$10n_r + 3M + \sqrt{M}/2 + 4$	$10n_r + 3M + \log(M) - 3$

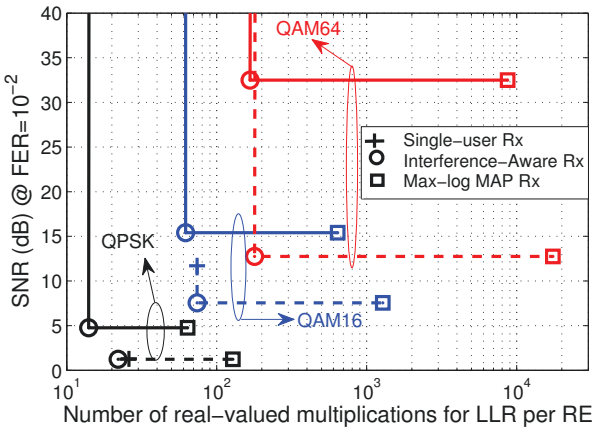

Figure 2 eNodeB has two antennas. Continuous lines indicate the case of single-antenna UEs while dashed lines indicate dual-antenna UEs. 3GPP LTE rate 1/2 punctured turbo code is used. Simulation settings are same as in the first part of Sec. 6.

information expressions for the case of finite alphabets have been relegated to Appendix A for simplicity and lucidity.

We focus on the LTE precoders but to analyze the degradation caused by the low-level quantization and the characteristic of EGT of these precoders, we also consider some other transmission strategies. Firstly, we consider unquantized MF precoder [23] that is given as

$$\mathbf{p} = \frac{1}{\sqrt{|h_{11}|^2 + |h_{21}|^2}} \begin{bmatrix} h_{11} \\ h_{21} \end{bmatrix} \tag{20}$$

For EGT, the unquantized MF precoder is given as

$$\mathbf{p} = \frac{1}{\sqrt{2}} \begin{bmatrix} 1 \\ h_{11}^* h_{21} / |h_{11}||h_{21}| \end{bmatrix} \tag{21}$$

To be fair in comparison with the geometric scheduling algorithm for multi-user MIMO in LTE, we introduce a geometric scheduling algorithm for unquantized precoders. We divide the spatial space into four quadrants according to the spatial angle between $\mathbf{h}_1^\dagger$ and $\mathbf{h}_2^\dagger$, which is given as

$$\phi = \cos^{-1}\left(\frac{\left|\mathbf{h}_1^\dagger \mathbf{h}_2\right|}{||\mathbf{h}_1||\,||\mathbf{h}_2||}\right) \qquad 0^\circ \le \phi \le 90^\circ \tag{22}$$

The geometric scheduling algorithm ensures that the eNodeB chooses the second UE to be served on the same RE as the first UE such that their channels $\mathbf{h}_1^\dagger$ and $\mathbf{h}_2^\dagger$ lie in the opposite quadrants.

Figure 3 shows the sum rates of a broadcast channel with the dual-antenna eNodeB and two single-antenna UEs for QAM64 alphabets. SNR is the transmit SNR, i.e., $\frac{\sigma_1^2||\mathbf{p}_1||^2 + \sigma_2^2||\mathbf{p}_2||^2}{N_0}$ whereas the two UEs have

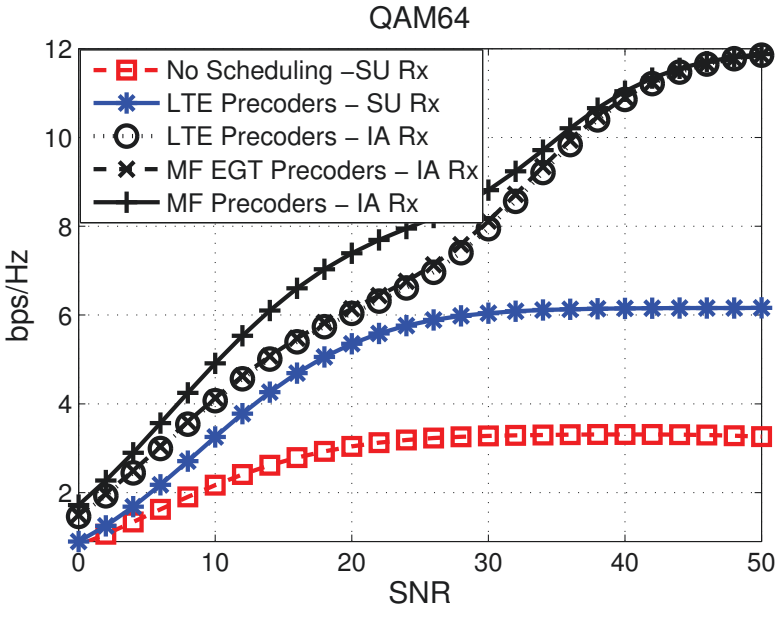

Figure 3 Sum rates of different transmission schemes for the downlink channel with dual-antenna eNodeB and 2 single-antenna UEs. 'No Scheduling - SU Rx' indicates the case once the eNodeB uses the LTE precoders without employing the geometric scheduling strategy. In all other cases, the eNodeB employs the geometric scheduling strategy along with the LTE precoders, MF EGT precoders and MF precoders. SU Rx indicates the cases when UEs employ single-user detection while IA Rx indicates the cases when UEs resort to the intelligent detection by employing the low-complexity interference-aware receivers.

equal-power distribution, i.e., $\sigma_1^2 = \sigma_2^2$, MF and MF EGT precoders are the unquantized precoders given in (20) and (21), respectively, while LTE precoders are the quantized precoders given in (1). The sum rates of unquantized precoders along with those of LTE quantized precoders are shown for the case of single-user receivers and for the case of low-complexity interference-aware receivers. The results show that under the proposed transmission strategy, the sum rate can be significantly improved (unbounded in SNR) if the low-complexity interference-aware receivers are used as compared to the case when the UEs resort to sub-optimal single-user detection where rates are bounded (in SNR). The behavior of single-user detection is attributed to the fact that this detection strategy considers interference as noise so the SINR is low once no geometric scheduling has been employed by the eNodeB while the SINR improves due to the reduction of interference once geometric scheduling is employed. However, the rates remain bounded in the SNR if the UEs resort to the single-user detection that is due to the fact that increasing the SNR (transmit SNR) also increases the interference strength thereby bounding the SINR at high values of the transmit SNR. On the other hand, there is significant improvement in the sum rate once UEs resort to intelligent detection by employing the low-complexity interference-aware receivers. In this case, the sum rate is unbounded if the rate (constellation size) of each UE is adapted with the SNR. Note that the quantized CSIT (LTE precoders) appears to have no effect at high SNR once UEs resort to intelligent interference-aware detection. This behavior is because the rate is not adapted with the SNR in these simulations, i.e., the constellation size is fixed to QAM64 and is not increased with the increase in the SNR. At high SNR, the rate of each UE gets saturated to its constellation size (six bits for QAM64) if the UE resorts to intelligent interference-aware detection. However, the approach to this saturation point (slope of the rate curve) depends on the quantization of channel information.

Another interesting result is the effect of the two characteristics of LTE precoders, i.e., low resolution and EGT. There is a slight improvement in the sum rate at medium SNR when the restriction of low resolution (LTE quantized precoders) is relaxed, i.e., eNodeB employs MF EGT precoders; however, there is a significant improvement in the sum rate when the restriction of EGT is eliminated, i.e the eNodeB employs MF precoders. This shows that the loss in spectral efficiency due to the employment of LTE precoders is mainly attributed to the EGT rather than their low resolution (quantization).

5. Performance analysis

We now focus on the EGT characteristic of the LTE precoders and carry out the performance analysis of the EGT in single-user and multi-user MIMO systems. We restrict to the case of single-antenna UEs while the eNodeB has two antennas. For single-user case, the received signal at the k-th RE is given by

$$y_{1,k} = \mathbf{h}_{1,k}^{\dagger}\mathbf{p}_{1,k}x_{1,k} + z_{1,k} \tag{23}$$

For EGT, the precoder vector is given by $\mathbf{p}_{1,k} = \frac{1}{\sqrt{2}}\begin{bmatrix} 1 & \frac{h_{21,k}h_{11,k}^*}{|h_{21,k}||h_{11,k}|} \end{bmatrix}^T$. So the received signal after normalization by $\frac{h_{11,k}}{|h_{11,k}|}$ is given by

$$y_{1,k}^N = \frac{1}{\sqrt{2}}(|h_{11,k}| + |h_{21,k}|)x_{1,k} + \frac{h_{11,k}}{|h_{11,k}|}z_{1,k} \tag{24}$$

where $y_{1,k}^N = \frac{h_{11,k}}{|h_{11,k}|}y_{1,k}$. The PEP has been derived in Appendix B and is given as

$$P(\underline{\mathbf{c}}_1 \to \hat{\underline{\mathbf{c}}}_1) \leq \frac{1}{2}\prod_{d_{\text{free}}}\left(\frac{48}{\left(\breve{d}_{1,\min}^2\left(\frac{\sigma_1^2}{N_0}\right)\right)^2}\right) \tag{25}$$

where $\breve{d}_{1,\min}^2$ is the normalized minimum distance of the constellation χ_1, d_{free} is the free distance (minimum Hamming distance) of the code. Note that $\underline{\mathbf{c}}_1$ and $\hat{\underline{\mathbf{c}}}_1$ are the correct and error codewords, respectively. Eq. 25 clearly shows full diversity of the EGT for single-user MIMO. Note that this result was earlier derived in [16] but was restricted to the case of BPSK. The same result was derived in [17] for EGT in MIMO systems using the approach of metrics of diversity order. Here, we have generalized this result and have adopted the natural approach of pairwise error probability to show the diversity order. Analysis of the EGT for multi-user MIMO system seemingly does not have closed form solution so we shall resort to the simulations for its analysis in Sec. 6.

6. Simulation results

Simulations are divided into three parts. In the first part, we look at the performance of the proposed interference-aware receiver structure for the multi-user MIMO mode in LTE while second part is dedicated to the sensitivity analysis of this receiver structure to the knowledge of the constellation of interference. This sensitivity analysis is motivated by the fact that the DCI formats in

the transmission mode 5 (multi-user MIMO) do not include the information of the constellation of the co-scheduled UE. Third part looks at the diversity order of the EGT in both single-user and multi-user MIMO modes in LTE.

For the first part (Figures 4 and 5), we consider the downlink of 3GPP LTE that is based on BICM OFDM transmission from the eNodeB equipped with two antennas using rate-1/3 LTE turbo code [24] with rate matching to rate 1/2 and 1/4. We deliberate on both the cases of single and dual-antenna UEs. We consider an ideal OFDM system (no ISI) and analyze it in the frequency domain where the channel has iid Gaussian matrix entries with unit variance and is independently generated for each channel use. We assume no power control in the multi-user MIMO mode so two UEs have equal-power distribution. Furthermore, all mappings of the coded bits to QAM symbols use Gray encoding. We focus on the FER while the frame length is fixed to 1,056 information bits. As a reference, we consider the fall-back transmit diversity scheme (LTE mode 2–Alamouti code) and compare it with the single-user and multi-user MIMO modes employing single-user receivers and low-complexity interference-aware receivers. To analyze the degradation caused by the low resolution and EGT of LTE precoders, we also look at the system

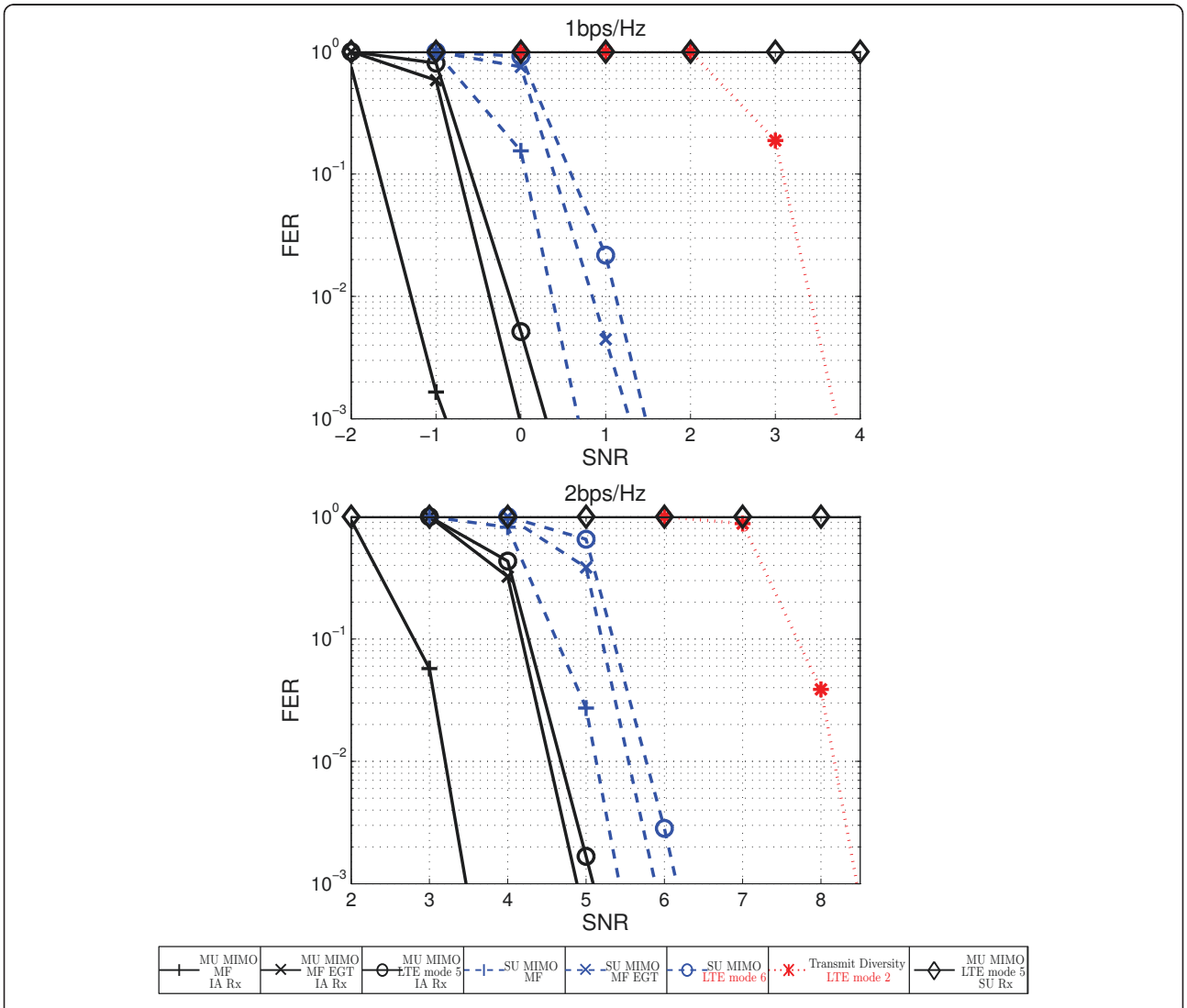

Figure 4 Downlink fast fading channel with the dual-antenna eNodeB and two single-antenna UEs. IA Rx indicates the low-complexity interference-aware receiver while SU Rx indicates the single-user receiver. MU MIMO and SU MIMO indicate multi-user and single-user MIMO, respectively. To be fair in comparison among different schemes, sum rates are fixed, i.e., if two users are served with QPSK with rate 1/2 in the multi-user mode, then one user is served with QAM16 with rate 1/2 in the single-user mode thereby equating the sum rate in both cases to 2 bps/Hz. 3GPP LTE rate 1/3 turbo code is used with different puncturing patterns.

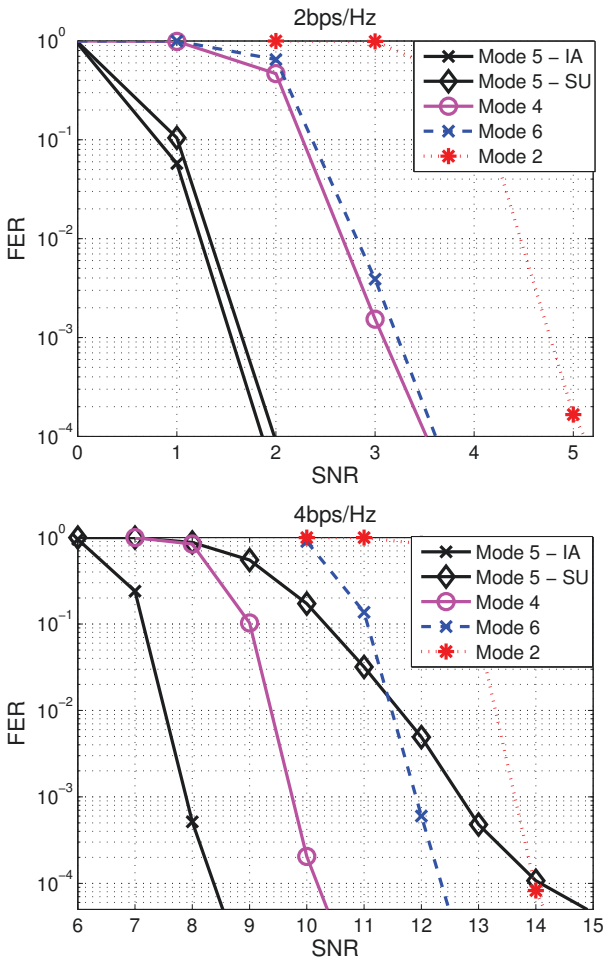

Figure 5 Downlink fast fading channel with the dual-antenna eNodeB and two dual-antenna UEs. IA indicates the low-complexity interference-aware receiver while SU indicates the single-user receiver. 3GPP LTE rate 1/3 turbo code is used with different puncturing patterns.

performance employing the unquantized MF and unquantized MF EGT precoders. To be fair in the comparison of the LTE multi-user MIMO mode (mode 5) employing the geometric scheduling algorithm with the multi-user MIMO mode employing unquantized MF and MF EGT precoders, we consider the geometric scheduling algorithm (Sec. 4) based on the spatial angle between the two channels (22). Perfect CSIT is assumed for the case of MF and MF EGT precoding while error free feedback of two bits (PMI) to the eNodeB is assumed for LTE precoders. It is assumed that the UE has knowledge of the constellation of co-scheduled UE in the multi-user MIMO mode. It is further assumed that the UE knows its own channel from the eNodeB. So in multi-user MIMO mode, the UE can find the effective interference channel based on the fact that the eNodeB schedules the second UE on the same RE whose precoder is 180° out of phase of the precoder of the first UE. Figure 4 shows the results for the case of single-antenna UEs. It shows enhanced performance of the multi-user MIMO mode once the UEs resort to intelligent detection by employing the low-complexity interference-aware receivers. The performance is severely degraded once the UEs resort to single-user detection. An interesting result is almost the equivalent performance of the unquantized MF EGT and low-resolution LTE precoders, which shows that the loss with respect to the unquantized CSIT is attributed to the EGT rather than the low resolution of LTE precoders. Performance degradation is observed for LTE multi-user MIMO mode for higher spectral efficiencies. Figure 5 shows the results for the case of dual-antenna UEs and focuses on different LTE modes employing LTE precoders. It shows that single-user detection performs close to interference-aware detection at low spectral efficiencies once UE has two antennas; however, its performance degrades at higher spectral efficiencies. This behavior is attributed to the fact that the rate with single-user detection gets saturated at high SNR due to the increased interference strength as was shown in Sec. 4. So the performance of single-user detection degrades for high spectral efficiencies as these spectral efficiencies are higher than the rate or mutual information of the single-user detection. For single-user MIMO (Mode 6), there is no saturation of the rate at high SNR as there is no interference. So mode 6 performs better than mode 5 at high SNR for higher spectral efficiencies once UEs employ single-user detection. However, if UEs resort to the intelligent interference-aware detection, the multi-user MIMO mode shows enhanced performance over other transmission modes in LTE. No degradation of LTE multi-user MIMO mode is observed at higher spectral efficiencies once UEs have receive diversity (dual antennas).

In the second part of simulations, we look at the sensitivity of the proposed receiver structure to the knowledge of the constellation of co-scheduled UE for the multi-user MIMO mode in LTE. The simulation settings are same as of the first part except that we consider the case when UE has no knowledge of the constellation of co-scheduled UE. The UE assumes this unknown interference constellation to be QPSK, QAM16, or QAM64, and the results for these different assumptions are shown in Figure 6. Results show that there is negligible degradation in the performance of the proposed receiver if the interfering constellation is assumed to be QAM16 or QAM64. However, there is significant degradation if the interference is assumed to be QPSK when it actually comes from QAM64. It indicates that assuming interference to be from a higher order modulation among the possible modulation alphabets leads to the best

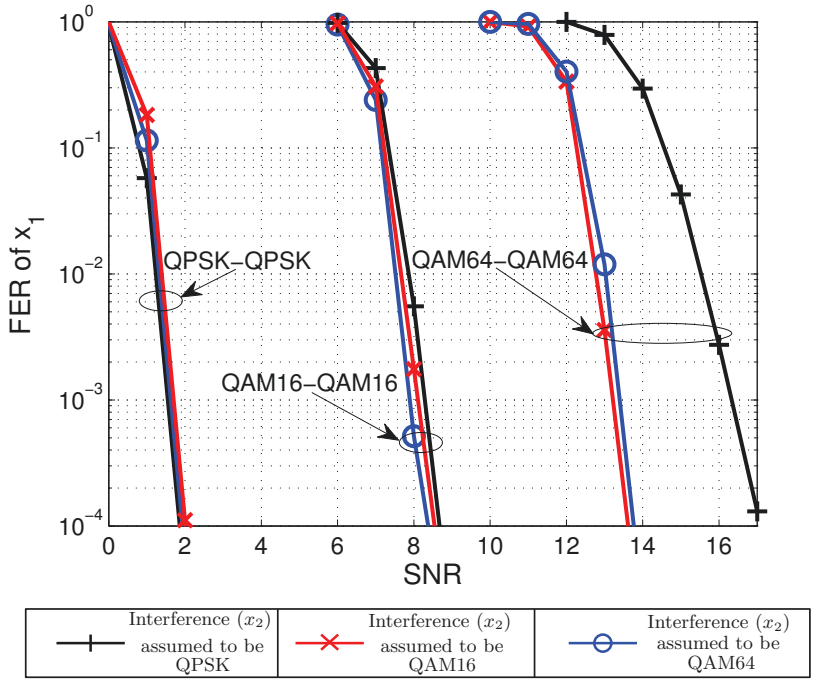

Figure 6 Interference sensitivity for the multi-user MIMO mode in LTE. Three sets of simulations are shown. QPSK-QPSK indicates that both x_1 and x_2 belong to QPSK. UE-1 does not know the constellation of interference (x_2) and assumes it to be QPSK, QAM16, and QAM64.

compromise as this assumption includes the lower modulation orders as special cases (with proper scaling). However, the converse is not true, i.e., assuming interference from lower modulation order cannot include higher order modulations. As LTE and LTE-Advanced restrict the transmission to three modulations (QPSK, QAM16, and QAM64), assuming interference to be QAM64 (or even QAM16) leads to better performance. The proposed receiver structure, therefore, can still exploit the discrete nature of the interference even if it does not know its modulation order. As the complexity of this receiver structure is independent of the constellation of interference, the assumption of higher order modulation does not add to the complexity of detection.

In the third set of simulations, we look at the diversity order of the single-user MIMO and multi-user MIMO schemes in LTE. The system settings are same as in the first part, but now we consider slow fading environment, i.e., the channel remains constant for the duration of one codeword. Figure 7 shows that the MF precoders have full diversity both in multi-user MIMO and single-user MIMO modes. However, once the constraint of EGT is imposed on the MF precoders, multi-user MIMO mode loses diversity while single-user MIMO still exhibits full diversity, which is in conformity with the analytical results of Sec. 5. This fundamental result holds even when the low-level quantization of LTE is imposed on these EGT precoders. Earlier conclusion that the performance loss in the multi-user MIMO mode in LTE is attributed to the EGT rather than the low resolution of LTE precoders is further confirmed. These results give a general guideline for the possible employment of the single-user MIMO and multi-user MIMO in LTE under different environments. Once not enough diversity is available in the channel, single-user MIMO is the preferred option while multi-user MIMO is the possible choice once the channel is rich in diversity.

7. Design of LTE precoder codebook with additional feedback

It was shown in the information theoretic analysis and was subsequently confirmed in the simulations that the loss in spectral efficiency due to the low-level quantized CSIT (LTE precoders) in the multi-user MIMO mode is more attributed to the EGT of the LTE codebook rather than its low resolution. It was also shown that EGT loses diversity in the multi-user MIMO mode. Focusing on these fundamental results, we now look at the design of the precoder codebook for future standardizations of LTE. Feedback of CSIT is expected to increase in these forthcoming wireless systems. However, the complexity associated with the feedback overhead combined with the low rate feedback channels would allow only a limited increase in the feedback. We therefore consider the case of two additional feedback bits for the quantized

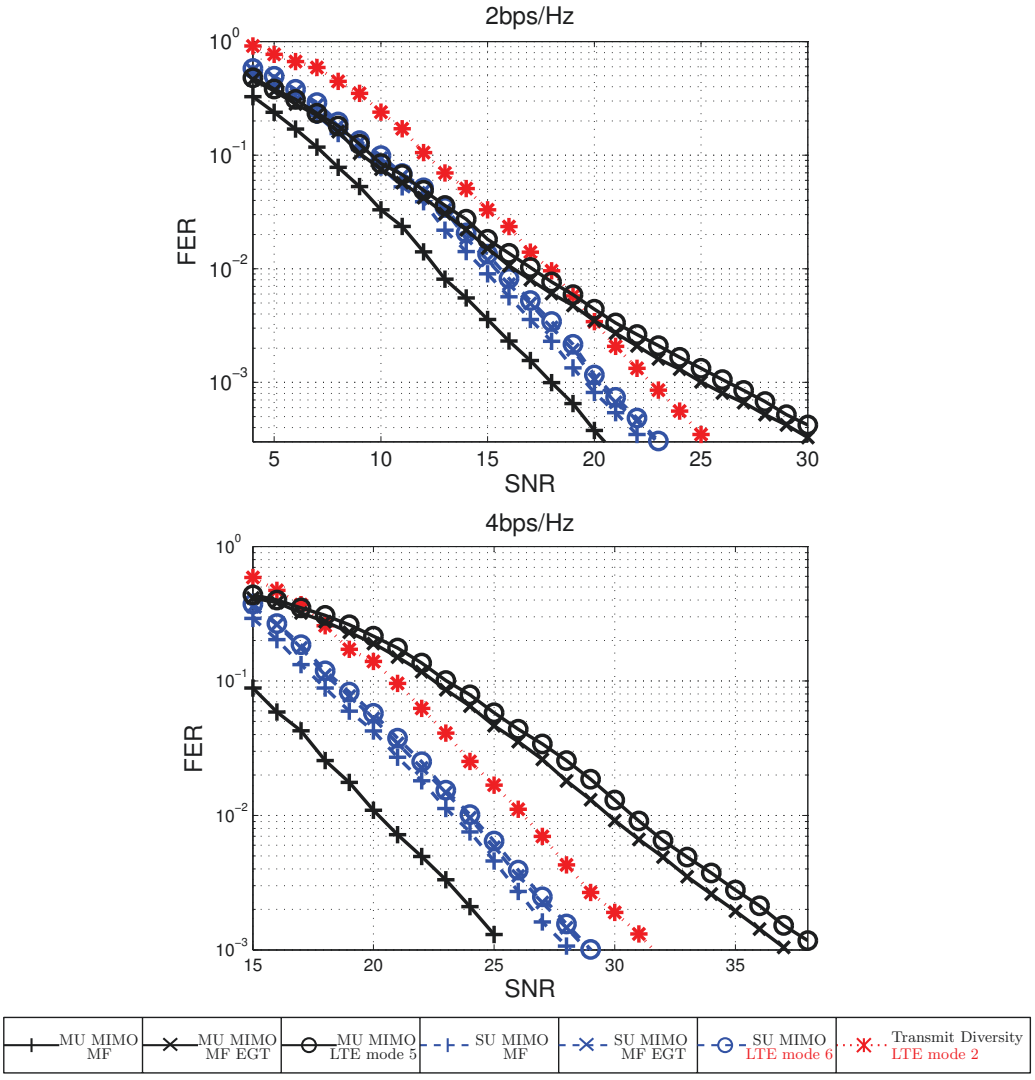

Figure 7 Diversity in the single-user and multi-user MIMO modes. Downlink slow fading channel (one channel realization per codeword) with dual-antenna eNodeB and two single-antenna UEs. 3GPP LTE rate 1/3 turbo code is used with different puncturing patterns.

CSIT (precoder codebook) and look how these additional bits can be efficiently employed.

We consider two options for the employment of these additional feedback bits as illustrated in Figure 8. As the LTE precoder is $[1\ \exp(j\theta)]^T$, so additional bits can be used to increase the angular resolution of θ, i.e., more points on the unit circle but restricting to EGT as shown in Figure 8a. Another option is to increase the levels of transmission, i.e., the additional feedback bits are used by the UE to indicate an increase of the power level on either of the two antennas as $[1\ 2\ \exp(j\theta)]^T$ or $[2\ \exp(j\theta)\ 1]^T$.

With this new precoding codebook design, the earlier described scheduling strategy remains same, i.e., for a UE to be scheduled in the multi-user MIMO mode, the eNodeB selects the second UE to be served on the same time-frequency resources (co-scheduled UE) such that the desired signal strength is maximized while interference strength is minimized for both the UEs. So if UE-1 has requested the precoder $\mathbf{p}_1$, the eNodeB finds the precoding vector $\mathbf{p}_2$ in the codebook, which minimizes their cross-correlation $(\mathbf{p}_1^{\dagger}\mathbf{p}_2)$ and then schedules the second UE with UE-1, which has requested $\mathbf{p}_2$ as its desired precoding vector. The receiver structure being independent of the codebook design also remains same for these new precoding codebooks.

We now look at the effect of two additional bits of feedback for PMI on the performance. We focus on the two options of improved angular resolution and additional levels of transmission. The simulation settings are same as of the previous section. Figure 9 illustrates the performance both in fast and slow fading channels.

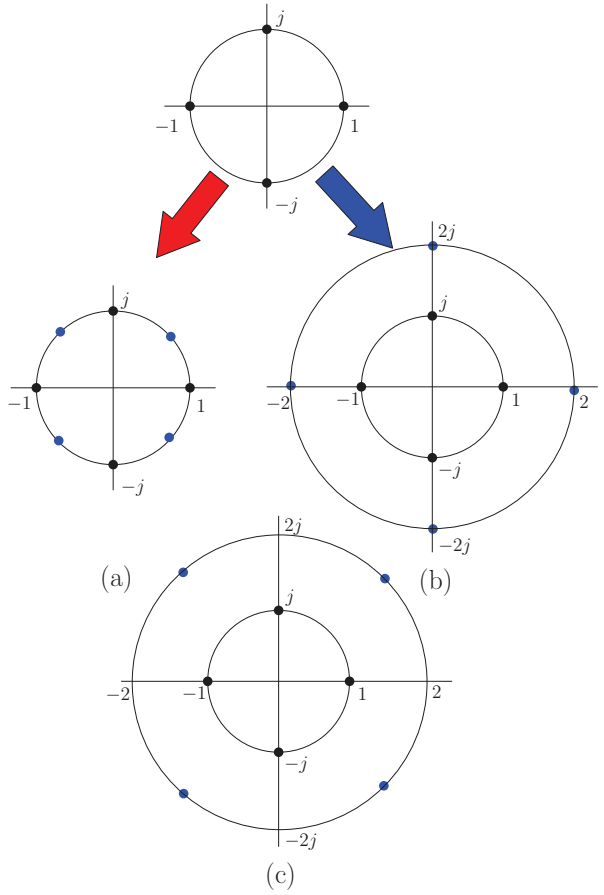

Figure 8 Two options of using two additional bits of feedback for PMI. Upper row corresponds to the option of increased angular resolution of LTE precoders while lower row corresponds to the option of enhanced levels of transmission. Square indicates the precoder entry for the first antenna while cross indicates the precoder entry for the second antenna.

These results show significant improvement in the performance of the multi-user MIMO mode when the additional feedback bits are employed to increase the levels of transmission as compared to the case of increasing the angular resolution. The performance is within 1.7 dB of the lower bound where lower bound is the performance curve for MF precoder without any interference. In slow fading environment, the change of the slope of FER curve with increased levels of transmission indicates improved diversity as compared to the case of increased angular resolution. On the other hand, little gain is observed in the single-user mode with additional feedback bits, which is expected as the standard LTE precoders have been optimized for the single-user transmission. These results indicate that the design of precoders for the forthcoming versions of LTE should consider increasing transmission levels rather than enhancing the angular resolution of the precoders. This proposed design is not merely restricted to the framework of LTE but gives fundamental design guidelines for precoding in modern wireless systems.

8. Conclusions

In this paper, we have looked at the feasibility of the multi-user MIMO for future wireless systems that are characterized by low-level quantization of CSIT. We have shown that multi-user MIMO can deliver its promised gains if the UEs resort to intelligent detection rather than the sub-optimal single-user detection. To this end, we have proposed a low-complexity interference-aware receiver structure that is characterized by the exploitation of the structure of residual interference. We have analyzed two important characteristics of the LTE precoders, i.e., low resolution and EGT. We have shown that the performance loss of the LTE precoders in the multi-user MIMO mode is attributed to their characteristic of EGT rather than their low resolution. We have further shown that the EGT is characterized by full diversity in the single-user MIMO mode but it loses diversity in the multi-user MIMO. Based on these fundamental results, we have proposed a design of the precoder codebook for forthcoming standardizations of LTE incorporating more levels of transmission.

Appendix A

Mutual information for finite alphabets

The mutual information for UE-1 for finite size QAM constellation with $|\chi_1| = M_1$ takes the form as

$$\begin{aligned} I\left(Y_1; X_1|\mathbf{h}_1^\dagger, \mathbf{P}\right) &= \mathcal{H}\left(X_1|\mathbf{h}_1^\dagger, \mathbf{P}\right) - \mathcal{H}\left(X_1|Y_1, \mathbf{h}_1^\dagger, \mathbf{P}\right) \\ &= \log M_1 - \mathcal{H}(X_1|Y_1, \mathbf{h}_1^\dagger, \mathbf{P}) \end{aligned} \tag{26}$$

where $\mathcal{H}(.) = -E\log p(.)$ is the entropy function. The second term of (26) is given as

$$\begin{aligned} \mathcal{H}(X_1|Y_1, \mathbf{h}_1^\dagger, \mathbf{P}) &= \sum_{x_1}\int_{y_1}\int_{\mathbf{h}_1^\dagger\mathbf{p}_1}\int_{\mathbf{h}_1^\dagger\mathbf{p}_2} p(x_1, y_1, \mathbf{h}_1^\dagger\mathbf{p}_1, \mathbf{h}_1^\dagger\mathbf{p}_2)\log\frac{1}{p(x_1|y_1, \mathbf{h}_1^\dagger\mathbf{p}_1, \mathbf{h}_1^\dagger\mathbf{p}_2)}\mathrm{d}y_1\mathrm{d}(\mathbf{h}_1^\dagger\mathbf{p}_1)\mathrm{d}(\mathbf{h}_1^\dagger\mathbf{p}_2) \\ &= \sum_{x_1}\sum_{x_2}\int_{y_1}\int_{\mathbf{h}_1^\dagger\mathbf{p}_1}\int_{\mathbf{h}_1^\dagger\mathbf{p}_2} p(x_1, x_2, y_1, \mathbf{h}_1^\dagger\mathbf{p}_1, \mathbf{h}_1^\dagger\mathbf{p}_2)\log\frac{\sum_{x_1'}\sum_{x_2'} p(y_1|x_1', x_2', \mathbf{h}_1^\dagger\mathbf{p}_1, \mathbf{h}_1^\dagger\mathbf{p}_2)}{\sum_{x_2'} p(y_1|x_1, x_2', \mathbf{h}_1^\dagger\mathbf{p}_1, \mathbf{h}_1^\dagger\mathbf{p}_2)}\mathrm{d}y_1\mathrm{d}(\mathbf{h}_1^\dagger\mathbf{p}_1)\mathrm{d}(\mathbf{h}_1^\dagger\mathbf{p}_2) \end{aligned} \tag{27}$$

where $x_1' \in \chi_1$ and $x_2' \in \chi_2$. Conditioned on the channel and the precoder, there is one source of randomness, i.e., noise. So (27) can be extended as

$$\begin{aligned} \mathcal{H}(X_1|Y_1, \mathbf{h}_1^\dagger, \mathbf{P}) &= \frac{1}{M_1M_2}\sum_{\mathbf{x}} E_{z_1}\log\frac{\sum_{\mathbf{x}'}\exp\left[-\frac{1}{N_0}\left|\mathbf{h}_1^\dagger\mathbf{p}_1x_1 + \mathbf{h}_1^\dagger\mathbf{p}_2x_2 + z_1 - \mathbf{h}_1^\dagger\mathbf{p}_1x_1' - \mathbf{h}_1^\dagger\mathbf{p}_2x_2'\right|^2\right]}{\sum_{x_2'}\exp\left[-\frac{1}{N_0}\left|\mathbf{h}_1^\dagger\mathbf{p}_2x_2 + z_1 - \mathbf{h}_1^\dagger\mathbf{p}_2x_2'\right|^2\right]} \\ &= \frac{1}{M_1M_2}\sum_{\mathbf{x}} E_{z_1}\log\frac{\sum_{\mathbf{x}'}\exp\left[-\frac{1}{N_0}\left|\mathbf{h}_1^\dagger\mathbf{P}(\mathbf{x}-\mathbf{x}') + z_1\right|^2\right]}{\sum_{x_2'}\exp\left[-\frac{1}{N_0}\left|\mathbf{h}_1^\dagger\mathbf{P}(\mathbf{x}-\mathbf{x}_2') + z_1\right|^2\right]} \end{aligned} \tag{28}$$

where $M_2 = |\chi_2|$, $\mathbf{x} = [x_1\ x_2]^T$, $\mathbf{x}' = [x_1'\ x_2']^T$ and $\mathbf{x}_2' = [x_1\ x_2']^T$. The mutual information for UE-1 can be rewritten as

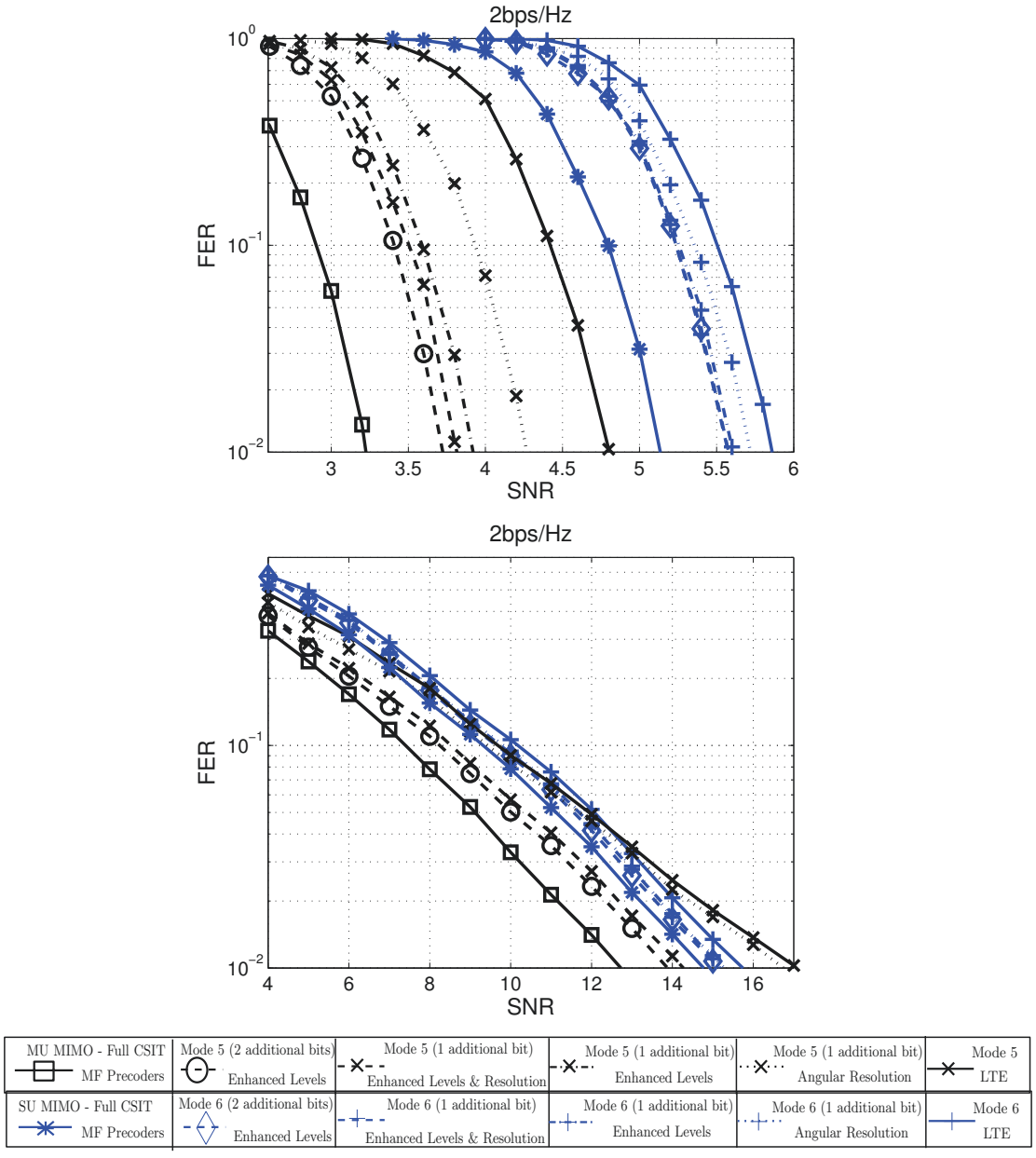

Figure 9 Proposed precoder codebook. Downlink channel with dual-antenna eNodeB and two single-antenna UEs. *Top figure* shows the results for fast fading channels while bottom figure illustrates the performance for slow fading channels. 3GPP LTE rate 1/3 turbo code is used with different puncturing patterns.

$$I(Y_1;X_1|\mathbf{h}_1^\dagger,\mathbf{P}) = \log M_1 - \frac{1}{M_1M_2}\sum_{\mathbf{x}} E_{z_1}\log\frac{\sum_{x'} p\left(y_1|\mathbf{x}',\mathbf{h}_1^\dagger,\mathbf{P}\right)}{\sum_{x_2'} p\left(y_1|\mathbf{x}_2',\mathbf{h}_1^\dagger,\mathbf{P}\right)} \quad (29)$$

$$\begin{aligned} I(Y;X_1|\mathbf{h}_1^\dagger\mathbf{p}_1,\mathbf{h}_1^\dagger\mathbf{p}_2) &= \log M_1 - \frac{1}{M_1M_2N_{z_1}N_{h_1}}\sum_{x_1}\sum_{x_2}\sum_{h_1}^{N_{h_1}}\sum_{z_1}^{N_{z_1}}\log\frac{\sum_{x_1'}\sum_{x_2'}\exp\left[-\frac{1}{N_0}\left|y_1-\mathbf{h}_1^\dagger\mathbf{p}_1x_1'-\mathbf{h}_1^\dagger\mathbf{p}_2x_2'\right|^2\right]}{\sum_{x_2'}\exp\left[-\frac{1}{N_0}\left|y_1-\mathbf{h}_1^\dagger\mathbf{p}_1x_1-\mathbf{h}_1^\dagger\mathbf{p}_2x_2'\right|^2\right]} \\ &= \log M_1 - \frac{1}{M_1M_2N_{z_1}N_{h_1}}\sum_{x_1}\sum_{x_2}\sum_{h_1}^{N_{h_1}}\sum_{z_1}^{N_{z_1}}\log\frac{\sum_{x_1'}\sum_{x_2'}\exp\left[-\frac{1}{N_0}\left|\mathbf{h}_1^\dagger\mathbf{p}_1x_1+\mathbf{h}_1^\dagger\mathbf{p}_2x_2+z_1-\mathbf{h}_1^\dagger\mathbf{p}_1x_1'-\mathbf{h}_1^\dagger\mathbf{p}_2x_2'\right|^2\right]}{\sum_{x_2'}\exp\left[-\frac{1}{N_0}\left|\mathbf{h}_1^\dagger\mathbf{p}_2x_2+z_1-\mathbf{h}_1^\dagger\mathbf{p}_2x_2'\right|^2\right]} \end{aligned} \quad (30)$$

The above quantities can be easily approximated using sampling (Monte-Carlo) methods with N_z realizations of noise and N_{h_1} realizations of the channel $\mathbf{h}_1^\dagger$ where the precoding matrix depends on the channel. So we can rewrite (29) as (30).

Similarly the mutual information for UE-2 is given as

$$I(Y_2;X_2|\mathbf{h}_2^\dagger,\mathbf{P}) = \log M_2 - \frac{1}{M_1M_2}\sum_{\mathbf{x}} E_{z_2}\log\frac{\sum_{x'} p\left(y_2|\mathbf{x}',\mathbf{h}_2^\dagger,\mathbf{P}\right)}{\sum_{x_1'} p\left(y_2|\mathbf{x}_1',\mathbf{h}_2^\dagger,\mathbf{P}\right)} \quad (31)$$

where $\mathbf{x}_1' = [x_1'\ x_2]^T$.

For the case of single-user MIMO mode, the mutual information is given by

$$I(Y_1; X_1|\mathbf{h}_1^\dagger, \mathbf{p}_1) = \log M_1 - \mathcal{H}\left(X_1|Y_1, \mathbf{h}_1^\dagger, \mathbf{p}_1\right) \tag{32}$$

where the second term is given by

$$\begin{aligned}\mathcal{H}\left(X_1|Y_1, \mathbf{h}_1^\dagger, \mathbf{p}_1\right) &= \sum_{x_1}\int_{y_1}\int_{\mathbf{h}_1^\dagger\mathbf{p}_1} p\left(x_1, y_1, \mathbf{h}_1^\dagger\mathbf{p}_1\right)\log\frac{1}{p\left(x_1|y_1, \mathbf{h}_1^\dagger\mathbf{p}_1\right)}\mathrm{d}y_1\mathrm{d}\left(\mathbf{h}_1^\dagger\mathbf{p}_1\right)\\ &= \sum_{x_1}\int_{y_1}\int_{\mathbf{h}_1^\dagger\mathbf{p}_1} p\left(x_1, y_1, \mathbf{h}_1^\dagger\mathbf{p}_1\right)\log\frac{\sum_{x_1'} p\left(y_1|x_1', \mathbf{h}_1^\dagger\mathbf{p}_1\right)}{p\left(y_1|x_1, \mathbf{h}_1^\dagger\mathbf{p}_1\right)}\mathrm{d}y_1\mathrm{d}\left(\mathbf{h}_1^\dagger\mathbf{p}_1\right)\\ &= \frac{1}{M_1 N_z N_{h_1}}\sum_{x_1}\sum_{\mathbf{h}_1^\dagger}^{N_{h_1}}\sum_{z_1}^{N_z}\log\frac{\sum_{x_1'}\exp\left[-\frac{1}{N_0}\left|y_1 - \mathbf{h}_1^\dagger\mathbf{p}_1 x_1'\right|^2\right]}{\exp\left[-\frac{1}{N_0}\left|y_1 - \mathbf{h}_1^\dagger\mathbf{p}_1 x_1\right|^2\right]}\end{aligned} \tag{33}$$

where N_{h_1} are the number of channel realizations of the channel $\mathbf{h}_1^\dagger$. Note that the precoding vector $\mathbf{p}_1$ is dependent on the channel $\mathbf{h}_1^\dagger$.

Appendix B

Diversity analysis of EGT in single-user MIMO

Consider the system equation 24, i.e.,

$$y_{1,k}^N = \frac{1}{\sqrt{2}}(|h_{11,k}| + |h_{21,k}|)x_{1,k} + \frac{h_{11,k}}{|h_{11,k}|}z_{1,k} \tag{34}$$

The max-log MAP bit metric [20] for the bit $c_{k'}$ can be written as

$$\Lambda_1^i(y_k, c_{k'}) \approx \min_{x_1\in\chi_{1,c_{k'}}^i}\left[\frac{1}{N_0}\left|y_{1,k}^N - \frac{1}{\sqrt{2}}(|h_{11,k}| + |h_{21,k}|)x_1\right|^2\right] \tag{35}$$

The conditional PEP i.e $P(\underline{\mathbf{c}}_1 \to \hat{\underline{\mathbf{c}}}_1|\mathbf{h}_1)$ is given as

$$\begin{aligned}P(\underline{\mathbf{c}}_1 \to \hat{\underline{\mathbf{c}}}_1|\bar{\mathbf{H}}_1) = P\Bigg(&\sum_k \min_{x_1\in\chi_{1,c_{k'}}^i}\frac{1}{N_0}\left|y_{1,k}^N - \frac{1}{\sqrt{2}}(|h_{11,k}| + |h_{21,k}|)x_1\right|^2\\ &\geq \sum_{k'}\min_{x_1\in\chi_{1,\hat{c}_{k'}}^i}\frac{1}{N_0}\left|y_{1,k}^N - \frac{1}{\sqrt{2}}(|h_{11,k}| + |h_{21,k}|)x_1\right|^2|\bar{\mathbf{H}}_1\Bigg)\end{aligned} \tag{36}$$

where $\bar{\mathbf{H}}_1$ indicates the complete channel from the eNodeB to UE-1 for the transmission of the codeword $\underline{\mathbf{c}}_1$. Assume $d(\underline{\mathbf{c}}_1 - \hat{\underline{\mathbf{c}}}_1) = d_{\text{free}}$ for $\underline{\mathbf{c}}_1$ and $\hat{\underline{\mathbf{c}}}_1$ under consideration for the PEP analysis, which is the worst case scenario between any two codewords. Therefore, the inequality on the right hand side of (36) shares the same terms on all but d_{free} summation points and the summations can be simplified to only d_{free} terms for which $\hat{c}_{k'} = \bar{c}_{k'}$. Let's denote

$$\begin{aligned}\tilde{x}_{1,k} &= \arg\min_{x_1\in\chi_{1,c_{k'}}^i}\frac{1}{N_0}\left|y_{1,k}^N - \frac{1}{\sqrt{2}}(|h_{11,k}| + |h_{21,k}|)x_1\right|^2\\ \hat{x}_{1,k} &= \arg\min_{x_1\in\chi_{1,\bar{c}_{k'}}^i}\frac{1}{N_0}\left|y_{1,k}^N - \frac{1}{\sqrt{2}}(|h_{11,k}| + |h_{21,k}|)x_1\right|^2\end{aligned} \tag{37}$$

As $\frac{1}{N_0}\left|y_{1,k}^N - \frac{1}{\sqrt{2}}(|h_{11,k}| + |h_{21,k}|)x_{1,k}\right|^2 \geq \frac{1}{N_0}\left|y_{1,k}^N - \frac{1}{\sqrt{2}}(|h_{11,k}| + |h_{21,k}|)\tilde{x}_{1,k}\right|^2$, this leads to PEP being given as

$$\begin{aligned}P(\underline{\mathbf{c}}_1 \to \hat{\underline{\mathbf{c}}}_1|\bar{\mathbf{H}}_1) &\leq P\Bigg(\sum_{k,d_{\text{free}}}\frac{1}{N_0}\left|y_{1,k}^N - \frac{1}{\sqrt{2}}(|h_{11,k}| + |h_{21,k}|)x_{1,k}\right|^2\\ &\qquad\geq \sum_{k,d_{\text{free}}}\frac{1}{N_0}\left|y_{1,k}^N - \frac{1}{\sqrt{2}}(|h_{11,k}| + |h_{21,k}|)\hat{x}_{1,k}\right|^2|\bar{\mathbf{H}}_1\Bigg)\\ &= P\Bigg(\sum_{k,d_{\text{free}}}\frac{\sqrt{2}(|h_{11,k}| + |h_{21,k}|)}{N_0}(z_{1,k}^*(\hat{x}_{1,k} - x_{1,k}))_R\\ &\qquad\geq \sum_{k,d_{\text{free}}}\frac{1}{2N_0}(|h_{11,k}| + |h_{21,k}|)^2|\hat{x}_{1,k} - x_{1,k}|^2\Bigg)\\ &= Q\left(\sqrt{\sum_{kd_{\text{free}}}\frac{1}{4N_0}(|h_{11,k}| + |h_{21,k}|)^2|(x_{1,k} - \hat{x}_{1,k})|^2}\right)\\ &\leq \frac{1}{2}\exp\left(-\sum_{k,d_{\text{free}}}\frac{1}{8N_0}(|h_{11,k}| + |h_{21,k}|)^2 d_{1,\min}^2\right)\\ &= \frac{1}{2}\prod_{k,d_{\text{free}}}\exp\left(-\frac{1}{8N_0}(|h_{11,k}| + |h_{21,k}|)^2 d_{1,\min}^2\right)\end{aligned} \tag{38}$$

where we have used Chernoff bound $Q(x) \leq \frac{1}{2}\exp\left(\frac{-x^2}{2}\right)$. Averaging over channel leads to

$$\begin{aligned}P(\underline{\mathbf{c}}_1 \to \hat{\underline{\mathbf{c}}}_1) &\leq \frac{1}{2}E_{\bar{\mathbf{H}}_1}\prod_{k,d_{\text{free}}}\exp\left(-\frac{1}{8N_0}(|h_{11,k}| + |h_{21,k}|)^2 d_{1,\min}^2\right)\\ &= \frac{1}{2}\prod_{k,d_{\text{free}}}E_{\mathbf{h}_{1,k}}\exp\left(\left(-\frac{\breve{d}_{1,\min}^2}{4}\right)\frac{(|h_{11,k}| + |h_{21,k}|)^2\sigma_1^2}{2N_0}\right)\end{aligned} \tag{39}$$

Eq. 39 follows from the channel independence at each RE that is the consequence of the interleaving operation. Here we have used the notation $d_{1,\min}^2 = \sigma_1^2\breve{d}_{1,\min}^2$ with $\breve{d}_{1,\min}^2$ being the normalized minimum distance of the constellation χ_1. Using the moment generating function (MGF) of the SNR at the output of two branch EGC as per equations (2) and (23) in [25], PEP at high SNR is upper bounded as

$$\begin{aligned}P(\underline{\mathbf{c}}_1 \to \hat{\underline{\mathbf{c}}}_1) \leq \frac{1}{2}\prod_{d_{\text{free}}}\Bigg(&\frac{8\left(\frac{\sigma_1^2}{N_0}\right)^2 + \breve{d}_{1,\min}^2\left(\frac{\sigma_1^2}{N_0}\right)^3}{4\left(\frac{\sigma_1^2}{N_0}\right)^2\left(2 + \frac{\sigma_1^2\breve{d}_{1,\min}^2}{4N_0}\right)^2} - \frac{\left(\frac{\breve{d}_{1,\min}^2}{2\sqrt{2}}\right)\left(\frac{\sigma_1^2}{N_0}\right)}{\left(2 + \frac{\breve{d}_{1,\min}^2}{2}\left(\frac{\sigma_1^2}{N_0}\right)\right)^{3/2}}\\ &\times\left[\pi - 2\sin^{-1}\left(\sqrt{\frac{\left(\frac{\sigma_1^2}{N_0}\right)^{-1} + \frac{\breve{d}_{1,\min}^2}{4}}{2\left(\frac{\sigma_1^2}{N_0}\right)^{-1} + \frac{\breve{d}_{1,\min}^2}{4}}}\right)\right]\\ &+ \frac{4\left(\frac{\sigma_1^2}{N_0}\right)^2\left(4 + \frac{\breve{d}_{1,\min}^2}{2}\left(\frac{\sigma_1^2}{N_0}\right)\right)}{4\left(\frac{\sigma_1^2}{N_0}\right)^2\left(2 + \frac{\breve{d}_{1,\min}^2}{4}\left(\frac{\sigma_1^2}{N_0}\right)\right)^2\left(2 + \frac{\breve{d}_{1,\min}^2}{2}\left(\frac{\sigma_1^2}{N_0}\right)\right)}\Bigg)\end{aligned} \tag{40}$$

Using the identity $\cos^{-1}(x) = \frac{\pi}{2} - \sin^{-1}(x)$, we have

$$\pi - 2\sin^{-1}\left(\sqrt{\frac{\left(\frac{\sigma_1^2}{N_0}\right)^{-1} + \frac{\breve{d}_{1,\min}^2}{4}}{2\left(\frac{\sigma_1^2}{N_0}\right)^{-1} + \frac{\breve{d}_{1,\min}^2}{4}}}\right) = 2\cos^{-1}\left(\sqrt{\frac{\left(\frac{\sigma_1^2}{N_0}\right)^{-1} + \frac{\breve{d}_{1,\min}^2}{4}}{2\left(\frac{\sigma_1^2}{N_0}\right)^{-1} + \frac{\breve{d}_{1,\min}^2}{4}}}\right) \quad (41)$$

Taylor series expansion [26] of $\cos^{-1}(\sqrt{x})$ is given as

$$\cos^{-1}(\sqrt{x}) = \sqrt{2 - 2\sqrt{x}}\sum_{k=0}^{\infty}\frac{(1-\sqrt{x})^k(1/2)_k}{2^k(k! + 2kk!)} \quad \text{for } |-1+\sqrt{x}| < 2$$

where $x!$ is the factorial of x while $(x)_n$ is the Pochhammer symbol, i.e., $(x)_n = x\ (x+1)\ \ldots\ (x+n-1)$. For x closer to 1, a case that shall be occurring at high SNR in (41), first term will be dominant, i.e.,

$$\cos^{-1}\left(\sqrt{\frac{\left(\frac{\sigma_1^2}{N_0}\right)^{-1} + \frac{\breve{d}_{1,\min}^2}{4}}{2\left(\frac{\sigma_1^2}{N_0}\right)^{-1} + \frac{\breve{d}_{1,\min}^2}{4}}}\right) \approx \sqrt{2 - 2\sqrt{\frac{\left(\frac{\sigma_1^2}{N_0}\right)^{-1} + \frac{\breve{d}_{1,\min}^2}{4}}{2\left(\frac{\sigma_1^2}{N_0}\right)^{-1} + \frac{\breve{d}_{1,\min}^2}{4}}}} \quad (42)$$

Taylor series expansion of $\sqrt{x}$ at $x = 1$ is

$$\sqrt{x} = 1 + \frac{x-1}{2} - \frac{(x-1)^2}{8} + \frac{(x-1)^3}{16} - \cdots$$

In the expansion of $\sqrt{\frac{\left(\frac{\sigma_1^2}{N_0}\right)^{-1} + \frac{\breve{d}_{1,\min}^2}{4}}{2\left(\frac{\sigma_1^2}{N_0}\right)^{-1} + \frac{\breve{d}_{1,\min}^2}{4}}}$, first two terms will be dominant at high SNR thereby leading to

$$\begin{aligned}\sqrt{2 - \sqrt{\frac{\left(\frac{\sigma_1^2}{N_0}\right)^{-1} + \frac{\breve{d}_{1,\min}^2}{4}}{2\left(\frac{\sigma_1^2}{N_0}\right)^{-1} + \frac{\breve{d}_{1,\min}^2}{4}}}} &\approx \sqrt{2 - 2\left(1 + \frac{\frac{\left(\frac{\sigma_1^2}{N_0}\right)^{-1} + \frac{\breve{d}_{1,\min}^2}{4}}{2\left(\frac{\sigma_1^2}{N_0}\right)^{-1} + \frac{\breve{d}_{1,\min}^2}{4}} - 1}{2}\right)} \\ &= \sqrt{-\left(\frac{\left(\frac{\sigma_1^2}{N_0}\right)^{-1} + \frac{\breve{d}_{1,\min}^2}{4}}{2\left(\frac{\sigma_1^2}{N_0}\right)^{-1} + \frac{\breve{d}_{1,\min}^2}{4}} - 1\right)} \\ &= \frac{1}{\sqrt{2 + \frac{\breve{d}_{1,\min}^2}{4} + \left(\frac{\sigma_1^2}{N_0}\right)}}\end{aligned} \quad (43)$$

So rewriting (40), we get

$$\begin{aligned}P(\underline{\mathbf{c}}_1 \to \hat{\underline{\mathbf{c}}}_1) \le \frac{1}{2}\prod_{d_{\text{free}}}\Bigg(&\frac{2}{\left(2 + \frac{\breve{d}_{1,\min}^2}{4}\left(\frac{\sigma_1^2}{N_0}\right)\right)^2} + \frac{\breve{d}_{1,\min}^2\left(\frac{\sigma_1^2}{N_0}\right)}{4\left(2 + \frac{\breve{d}_{1,\min}^2}{4}\left(\frac{\sigma_1^2}{N_0}\right)\right)^2} \\ &- \frac{2\left(\frac{\breve{d}_{1,\min}^2}{2\sqrt{2}}\right)\left(\frac{\sigma_1^2}{N_0}\right)}{\left(2 + \frac{\breve{d}_{1,\min}^2}{2}\left(\frac{\sigma_1^2}{N_0}\right)\right)^{3/2}\left(2 + \frac{\breve{d}_{1,\min}^2}{4}\left(\frac{\sigma_1^2}{N_0}\right)\right)^{1/2}} \\ &+ \frac{\left(4 + \frac{\breve{d}_{1,\min}^2}{2}\left(\frac{\sigma_1^2}{N_0}\right)\right)}{\left(2 + \frac{\breve{d}_{1,\min}^2}{4}\left(\frac{\sigma_1^2}{N_0}\right)\right)^2\left(2 + \frac{\breve{d}_{1,\min}^2}{2}\left(\frac{\sigma_1^2}{N_0}\right)\right)}\Bigg)\end{aligned} \quad (44)$$

At high SNR, second term converges to $\frac{4}{\breve{d}_{1,\min}^2\left(\frac{\sigma_1^2}{N_0}\right)}$ while the third term converges to $\frac{-4}{\breve{d}_{1,\min}^2\left(\frac{\sigma_1^2}{N_0}\right)}$. So PEP at high SNR is upper bounded as

$$\begin{aligned}P(\underline{\mathbf{c}}_1 \to \hat{\underline{\mathbf{c}}}_1) &\le \frac{1}{2}\prod_{d_{\text{free}}}\left(\frac{32}{\left(\breve{d}_{1,\min}^2\left(\frac{\sigma_1^2}{N_0}\right)\right)^2} + \frac{16}{\left(\breve{d}_{1,\min}^2\left(\frac{\sigma_1^2}{N_0}\right)\right)^2}\right) \\ &= \frac{1}{2}\prod_{d_{\text{free}}}\left(\frac{48}{\left(\breve{d}_{1,\min}^2\left(\frac{\sigma_1^2}{N_0}\right)\right)^2}\right)\end{aligned} \quad (45)$$

Acknowledgements
Eurecom's research is partially supported by its industrial partners: BMW, Bouygues Telecom, Cisco Systems, France Télécom, Hitachi Europe, SFR, Sharp, ST Microelectronics, Swisscom, Thales. The research work leading to this paper has also been partially supported by the European Commission under SAMURAI and IST FP7 research network of excellence NEWCOM++.

Competing interests
The authors declare that they have no competing interests.

Received: 1 December 2010 Accepted: 14 July 2011
Published: 14 July 2011

References

1. IE Telatar, Capacity of multiantenna Gaussian channels. Eur Trans Telecommun. **10**(6), 585–595 (1999). doi:10.1002/ett.4460100604
2. D Gesbert, M Kountouris, R Heath, C-B Chae, T Salzer, Shifting the MIMO paradigm. IEEE Signal Process Mag. **24**(5), 36–46 (2007)
3. D Love, R Heath, V Lau, D Gesbert, B Rao, M Andrews, An overview of limited feedback in wireless communication systems. IEEE J Sel Areas Commun. **26**(8), 1341–1365 (2008)
4. LTE, *Evolved Universal Terrestrial Radio Access (E-UTRA); Physical Channels and Modulation, Release 8, V.8.6.0.* 3GPP TS 36.211 (2009)
5. S Sesia, I Toufik, M Baker, *LTE, The UMTS Long Term Evolution: From Theory to Practice* (Wiley, New York, 2009)
6. R Ghaffar, R Knopp, Linear precoders for multiuser MIMO for finite constellations and a simplified receiver structure under controlled interference, in *Asilomar Conference on Signals, Systems and Computers* (2009)
7. S Verdu, *Multiuser Detection* (Cambridge University Press, Cambridge, 1998)
8. L Brunel, Multiuser detection techniques using maximum likelihood sphere decoding in multicarrier CDMA systems. IEEE Trans Wirel Commun. **3**(3), 949–957 (2004). doi:10.1109/TWC.2004.827742
9. R Lupas, S Verdu, Linear multiuser detectors for synchronous code-division multiple-access channels. IEEE Trans Inf Theory. **35**(1), 123–136 (1989). doi:10.1109/18.42183
10. B Zarikoff, J Cavers, S Bavarian, An iterative groupwise multiuser detector for overloaded MIMO applications. IEEE Trans Wirel Commun. **6**(2), 443–447 (2007)
11. X Wang, H Poor, Iterative (turbo) soft interference cancellation and decoding for coded CDMA. IEEE Trans Commun. **47**(7), 1046–1061 (1999). doi:10.1109/26.774855
12. R de Lamare, R Sampaio-Neto, Minimum mean-squared error iterative successive parallel arbitrated decision feedback detectors for DS-CDMA systems. IEEE Trans Commun. **56**(5), 778–789 (2008)
13. JW Choi, A Singer, J Lee, NI Cho, Improved linear soft-input soft-output detection via soft feedback successive interference cancellation. IEEE Trans Commun. **58**(3), 986–996 (2010)
14. X Li, A Chindapol, J Ritcey, Bit-interleaved coded modulation with iterative decoding and 8 PSK signaling. IEEE Trans Commun. **50**(8), 1250–1257 (2002). doi:10.1109/TCOMM.2002.801524
15. M Speth, A Jansen, H Meyr, Iterative multiuser detection for bit interleaved coded modulation, in *IEEE International Conference on Communications, ICC 2000.* **2**, 894–898 (2000)
16. Q Zhang, Probability of error for equal-gain combiners over Rayleigh channels: some closed-form solutions. IEEE Trans Commun. **45**(3), 270–273 (1997). doi:10.1109/26.558680
17. D Love, R Heath Jr, Equal gain transmission in multiple-input multiple-output wireless systems. IEEE Trans Commun. **51**(7), 1102–1110 (2003). doi:10.1109/TCOMM.2003.814195
18. R Ghaffar, R Knopp, Diversity analysis of equal gain transmission for singleuser and multiuser MIMO, in *IEEE Global Communications Conference, Globecomm 2010,* Miami (Dec. 2010)
19. LTE, *Evolved Universal Terrestrial Radio Access (E-UTRA); Physical Layer Procedures, Release 8, V.8.6.0.* 3GPP TS 36.213 (2009)
20. G Caire, G Taricco, E Biglieri, Bit-interleaved coded modulation. IEEE Trans Inf Theory. **44**(3), 927–946 (1998). doi:10.1109/18.669123
21. S Alamouti, A simple transmit diversity technique for wireless communications. IEEE J Sel Areas Commun. **16**(8), 1451–1458 (1998). doi:10.1109/49.730453
22. R Ghaffar, R Knopp, Making Multiuser MIMO work for LTE, in *IEEE 21-st International Symposium on Personal, Indoor and Mobile Radio Communications (PIMRC 2010),* Istanbul (September 2010)
23. R Zakhour, ZKM Ho, D Gesbert, Distributed beamforming coordination in multicellular MIMO systems, in *IEEE 69th Vehicular Technology Conference, VTC-Spring. April, 26-29, 2009, Barcelona, Spain* (Dec. 2009)
24. LTE, Evolved Universal Terrestrial Radio Access (E-UTRA); Channel Coding and Multiplexing, Release 8, V.8.6.0. 3GPP TS 36.212 (2009)
25. X Qi, M-S Alouini, Y-C Ko, Closed-form analysis of dual-diversity equal-gain combining over Rayleigh fading channels. IEEE Trans Wirel Commun. **2**(6), 1120–1125 (2003). doi:10.1109/TWC.2003.819027
26. I Gradshteyn, I Ryzhik, *Table of Integrals, Series, and Products* (Academic Press, San Diego, 2000)

doi:10.1186/1687-1499-2011-40
Cite this article as: Ghaffar and Knopp: **Interference-aware receiver structure for multi-user MIMO and LTE.** *EURASIP Journal on Wireless Communications and Networking* 2011 **2011**:40.